



USE OF SILVER NANOPARTICLES MIXED WITH DEIONIZED WATER IN A RECTANGULAR TWO-PHASE CLOSED THERMOSYPHON: A CASE STUDY OF THE TWO-PHASE FLOW

Namphon Pipatpaiboon^a, Teerapat Chompookham^b, Sampan Rittidech^b, Yulong Ding^c, Thanya Parametthanuwat^d, Surachet Sichamnan^{a,*}

^a Department of Mechanical Engineering, Faculty of Industry and Technology, Rajamangala University of Technology Isan, Sakon Nakhon Campus, Sakon Nakhon 47160, Thailand

^b Heat Pipe and Thermal Tool Design Research Unit (HTDR), Division of Mechanical Engineering, Faculty of Engineering, Mahasarakham University, 44150, Thailand

^c Birmingham Centre for Thermal Energy Storage, School of Chemical Engineering, University of Birmingham, UK

^d Heat Pipe and Nanofluid Technology Research Unit, Faculty of Industrial Technology and Management, King Mongkut's University of Technology North Bangkok, 25230, Thailand

ABSTRACT

When nanofluid (NF) is used as the working fluid in a rectangular two-phase closed thermosyphon (RTPCT), the formations and heat performance of two-phase flow patterns are explored qualitatively. Silver nanoparticles were mixed with deionized water at a concentration of 0.5 wt% in the NF. Nanoparticles improved the thermal contact surface area within the base flow, allowing the base fluid to boil quickly and easily. When the working fluid was boiled, NF also demonstrated high thermal conductivity capabilities, which diffused and moved along with the dual flow patterns. As a result, these qualities improved the RTPCT's efficiency. Considering the findings of the RTPCT test at evaporation temperatures of 50, 70, and 90°C, three flow forms are observed: bubble flow (BF), slug flow (SF), and churn flow (CF), respectively. The slug flow (SF) and the churn flow (CF) are patterns that influence the heat flux. The greatest heat flow obtained from the test is 4.78 kW/m² at 90°C evaporation temperatures, whereas the heat flux measured at 70°C and 50°C evaporation temperatures is 2.95 kW/m² and 2.74 kW/m², respectively.

Keywords: Nanofluids, Internal flow, Flow pattern, Rectangular two-phase closed thermosyphon.

1. INTRODUCTION

Economic growth worldwide is mainly based on the progress made by the country's industrial sector. One significant system that drives industrial growth is the cooling system; therefore, heat exchangers that have high efficiencies are crucial for overall economic development. The two-phase closed thermosyphon (TPCT), a type of heat exchanger, has received considerable attention from researchers because of its high efficiency, which improves heat transfer. Also, a TPCT can be installed according to the dimensions of a site (Bhuwaketkumjohn and Parametthanuwat (2017)). A TPCT is a closed-end pipe that is welded on both sides; it is cylindrical with a round cross-sectional area. This research explored the shape adjustments of a TPCT based on its general appearance. Thus, the rectangular two-phase closed thermosyphon (RTPCT) was developed for filling NF as the working fluid. The RTPCT (see Figure 1) comprises three parts, namely, the evaporator section, the adiabatic section, and the condenser section. The pipes were made of copper, stainless steel, or carbon steel. The RTPCT works when the evaporator is heated by a heat source. Then, the received heat passes through from the pipe wall to the working fluid contained within the evaporator section. When the working fluid's temperature became higher than its saturated temperature, the working fluid was boiled and transformed from the liquid state into the vapor state.

Subsequently, vapor floats through the adiabatic section to the condenser section to release the heat. Condensation turns the working fluid from vapor into liquid form (Kew and Reay (2006), Noie et al. (2007) and Rittidech (2010)). Several researchers have recently performed thermosyphon experiments to explore and improve thermosyphon heat transmission capabilities and uses. These studies have involved changing the cross-sectional area, increasing the qualities of the functional chemicals, or researching the behaviors of two-state flow patterns created within the thermosyphon. Study of the thermal performance of a miniature heat pipe with a pipe cross-section for electronic devices and heat transfer processes. A computer's CPU was cooled using small heat pipes with square and triangular cross-sections. The length of the condenser section, adiabatic section, and evaporator section were 25, 15, and 10 mm, respectively. The results proved that small heat pipes with triangular cross-sectional areas provided higher heat resistance than pipes with square cross-sectional areas (Moon et al. (2004)). The changes in the shapes of the TPCT's cross-sectional area from round to flat were assessed based on different variables, such as the working fluid addition rate, heat feeding rate at the evaporator section, and the different aspect ratios. Water was used as the working fluid in this assessment.

* Corresponding author. Email: surachet.si@rmuti.ac.th

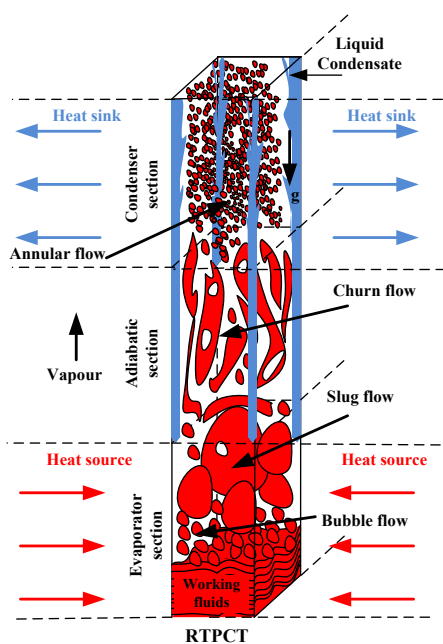


Fig. 1 The characteristics of RTPCT and the two-phase flow patterns

The results showed that a flat TPCT (FTPCT) has a higher average temperature in the evaporator section than a circular two-phase closed thermosyphon (CTPCT). When the heat fed to the evaporator was increased, it resulted in higher heat flux in all the test cases (Amatachaya and Srimuang (2010)). Heat pipes with circular, semicircular, and oval cross-sectional areas without porous materials were tested for the working fluids with filling ratios of 10%, 20%, and 30%. Here, water was used as the working fluid, and solar power collectors used had flat panels. The results revealed that for the working fluid with a filling ratio of 10%, the flat-paneled solar collector with an oval cross-sectional heat pipe (without porous material) showed better performance than a circular cross-sectional pipe. The working fluid had a filling ratio of 20%; the flat-paneled solar collector with an oval cross-sectional heat pipe (without porous material) showed lower efficiency than the heat pipes with oval and semicircular cross-sectional shapes (Hussein et al. (2006)). Changes in the cross-sectional area and fluid volumes from the CTPCT to the FTPCT directly affected the addition rate of the working fluid under the same working conditions. Thus, the working fluid at the evaporator section reached the boiling point quicker. This resulted in a better overall heat transfer rate in the FTPCT (Srimuang et al. (2009)). In addition, the thermal efficiency of the heat exchanger in the air conditioning system employing nanofluids. To lower the air conditioning system's energy usage The test revealed the maximum efficiency and thermal conductivity At 55°C intake air temperature and 1 m/s inlet air velocity, 0.59346 Watts and 883.284 Watts are equivalent, and the thermal recovery is 883.284 Watts. For the utilization of 5wt% CuO mass concentration while employing approximately 701.023 Watts of pure water in a nanofluid air conditioning system employing a heat exchanger. It conserves more energy than utilizing pure water (Abdallah et al. (2022)).

Assessments were conducted to evaluate the effects of using NF as a working fluid in the TPCT made from copper tubes with internal diameters of 7.5, 11.1, and 25.4 mm; the filling ratios were 30%, 50%, and 80% with respect to the evaporator volume, and the aspect ratios were 5, 10 and 20 in a vertical position. Also, the working temperatures were 40°C, 50°C, and 60°C. The results proved that for the aspect ratio of 20, the working temperature was 60°C, using NF as the working fluid in the TPCT with an internal diameter of 25.4 mm; the maximum heat transfer rate obtained was 750.81 W. This was 70% higher than when water was used as the working fluid (Paramethanuwat et al. (2010)). Using water mixed with silver nanoparticles as a working fluid within a heat pipe reduced the heat resistance within the pipe to

between 10% and 80% as compared with the situation when water alone was used as the working fluid and heat was transferred to the evaporator at 30–60 Watts. The heat resistance of HP decreased as the sizes of the silver nanoparticles and the concentrations increased. Changes in the cross-sectional area from the CTPCT to the FTPCT led to cross-sectional area and volume changes, which directly affected the addition rate of the working fluid under the same working conditions. Thus, the working fluid at the evaporator section heat reached the boiling point quicker. This resulted in a better overall heat transfer rate in the FTPCT (Kang et al. (2006)). The efficiency of the TPCT increased to 14.7% when aluminum oxide nanoparticles (Al_2O_3) were used as the working agent instead of deionized water. This efficiency increase was confirmed by the temperature distribution on the TPCT surface. One advantage of using fluid nanoparticles as the working fluid was the increase in the contact surface area where heat was received and emitted to the base liquid. Thus, the base liquid could be boiled easily when heated by the evaporator of the TPCT. Moreover, nanoparticles possess high thermal conductivity, which helped heat the pipe and the thermosyphon worked better as compared with the original base fluid (Noie et al. (2009)). The use of TiO_2 as the working fluid in the TPCT resulted in 1.4 times higher heat transfer efficiency when compared with the use of water as the working fluid (Shin et al. (2011)). Another factor that directly affected the heat transfer of the TPCT is the flow pattern of the two-phase working fluid generated by the heat cycle. The flow pattern behaviors included the nature of the occurrence of each type of flow that related to various variables, such as the working fluid, aspect ratio, pipe diameter, cross-sectional shape, inclination angle, filling ration of the working fluid and evaporator temperature. Previous studies have provided information on two-phase flow patterns, such as the use of R123 as the working fluid in a TPCT with an internal diameter of 11.1 mm. Assessments were conducted at 30°C of vapor temperature. The aspect ratios were 5, 10, and 30, and the filling ratio was 80% with respect to the evaporator volume; the inclination angles were 5°, 30°, and 90° from the horizontal plane. The results proved that at the aspect ratio of 30, the inclination angle was 90° from the horizontal plane, and the flux heat was 20.7 kW/m². The main flow patterns found were annular flow (AF) and churn flow (CF) combined with slug flow (SF). In the lower part of the evaporator, a bubble flow (BF) pattern was found, whereas the central and the upper parts of the evaporator showed SF, CF and AF respectively. Additionally, for the inclination angle of 30° from the horizontal plane and the heat flux of 24.6 kW/m², BF and SF were the main flow patterns. However, in the lower part of the evaporator, BF was observed. The central and upper parts of the evaporator section showed the SF with extended liquid wave and separated layer flow, respectively. At the inclination angle of 5° from the horizontal plane, the heat flux was 16.7 kW/m², and BF and SF were the main flow patterns found together with the slightly expanded liquid waves. The lower and middle parts of the evaporator section showed SF with liquid waves. The upper part of the evaporator section showed the SF pattern with liquid waves sprayed from the center of the evaporator. For every test having an aspect ratio of 10, the flow patterns created were similar to the flow patterns with the aspect ratio of 30. For the aspect ratio of 5, BF was the main flow pattern at the maximum heat flux values of 92.4, 78.6, and 53.9 kW/m² when the inclination angles were 30°, 90°, and 5°, respectively, from the horizontal plane (Terdtoon et al. (1998)).

In a previous study (Bhuwakietkumjohn and Rittidech (2010)), experiments were conducted on a circular oscillating heat pipe fitted with a nonreturn valve with an inner diameter of 2.4 mm, an inclination angle of 90° from the horizontal plane, and an evaporator temperature of 125°C; the results showed that the dispersed BF was in the lower part of the evaporator when using ethanol and ethanol mixed with silver nanoparticle powder as the working fluid. The maximum heat flux of 2.04 kW/m² was recorded when ethanol mixed with silver nanoparticle powder was used as the working fluid, whereas the maximum heat flux of 1.31 kW/m² was recorded when ethanol was used as the working fluid (Bhuwakietkumjohn and Rittidech (2010)). TPCTs made of glass

with graphene–acetone NF were used as the working fluids at concentrations of 0.05%, 0.07%, and 0.09%. When tested at 10, 20, 30, 40, and 50 W of heat applied at evaporator section, BF was found intermittently at 10 W; however, at 20 W, more BF was found. The CF was found when 30 W heat was applied. The CF changed to AF when the evaporator was heated to 40 and 50 W, and the AF resulted in the highest heat transfer coefficient. Additionally, heat resistance was reduced to a maximum of 70.3%, and the heat transfer coefficient of the evaporator increased to 61.25% at the concentration of 0.09% (Asirvatham et al. (2015)). The TPCT was made from a glass tubing with deionized water mixed with silver nanoparticles at the concentration of 0.5 wt% (NF) as the working fluid with respect to the total volume of water containing 1 wt% of oleic acid with respect to the total NF volume. Studies revealed four types of flow patterns: BF, SF, CF, and ring flow. Both the CF and ring flow influenced the heat transfer rate of the TPCT, which had an inner diameter of 7 mm at the inclination angles of 80° and 90°, respectively. For the TPCT with an inner diameter of 25.2 mm at the inclination angle of 80°, four types of flows were detected: BF, SF, CF, and a separate layer flow. The CF and the separate layer flow were found to affect the heat transfer rate. When testing the TPCT with the inner diameter of 25.2 mm at the inclination angle of 90°, four flow patterns were found, namely, BF, SF, CF, and turbulent flow. Turbulent flow occurred continuously when the temperature of the evaporator was increased from 70°C to 90°C. The CF and turbulent flow were found to affect the heat transfer rate in this test. Furthermore, the TPCT with inner diameters of 7 and 25.2 mm showed the highest heat transfer rates of 31.88 and 58.15 W, respectively, at the evaporator temperature of 90°C and the inclination angle of 80°C (Sichamnan et al. (2020)).

The two-phase flow patterns and the enhanced thermal efficiency limit of the RTPCT showed that the behavior and flow pattern were regulated by the structural characteristics of the pipes used to build the thermosyphon. Furthermore, the choice of modified working substances contributed to the flow pattern that transferred the heat from the evaporator to the condenser. This is considered an important behavior that improves the thermal efficiency of the thermosyphon design. Past research results showed a limited understating of the flow pattern of the RTPCT. Thus, this research focused on the behavior and characterization of the two-state flow patterns in which NF was used as a working substance with a two-state closed thermosyphon face area. The obtained data can be used as the basis for building, developing, and designing future RTPCTs.

2. THEORY AND ANALYSIS

2.1 Geometric characteristics of the cross – sectional adjustments

The basic principle of this study involved the different geometric cross-sectional theory (DGCST), as shown in Figure 2. The DGCST involves changes made to the cross-sectional area of RTPCT, as determined by the basic relationship of the TPCT. The determinants were the aspect ratio, cross-sectional area, wetted perimeter, and hydraulic radius (Srimuang et al. (2011)).

The aspect ratio can be obtained follows

$$\frac{T_e}{D_i} = \frac{L_e}{4R_h} \quad (1)$$

where T_e is the evaporator section length (m), D_i is the inner diameter of the pipe (m), and R_h is the hydraulic radius (m).

The cross-sectional area is obtained as follows

$$A = \frac{\pi Y^2}{4} + XY \quad (2)$$

where A is the cross - sectional area after modification (m²), X is the length of the pipe (m), and Y is the outer length of the pipe (m).

The wetted perimeter can be obtained as follows:

$$W_{perimeter} = \pi Y + XY \quad (3)$$

The hydraulic radius is given as follows:

$$R_h = \frac{(\pi / 4)Y^2 + XY}{\pi Y + 2X} \text{ which means } 4R_h = D_i \quad (4)$$

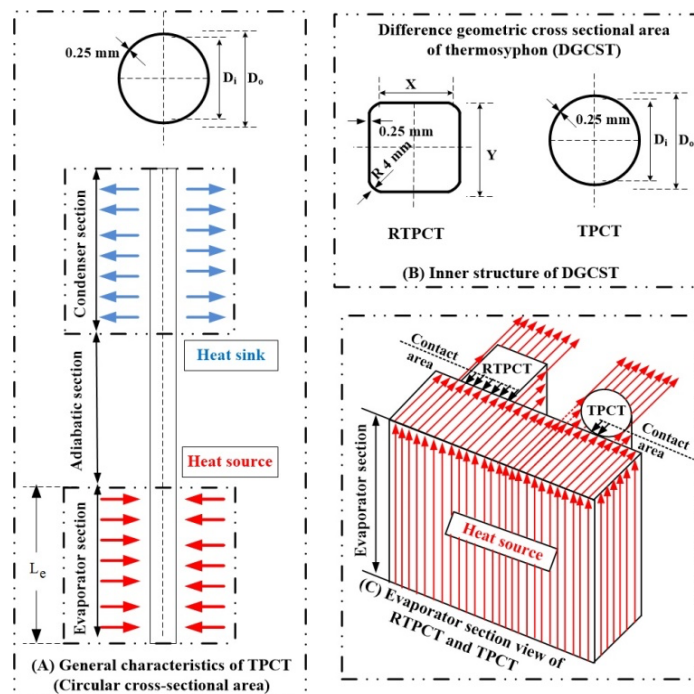


Fig. 2 Characteristics of cross-sectional geometry of RTPCT and TPCT

2.2 Preparation of silver nanoparticle fluid

To prepare silver nanoparticles <100 nm with a 99.9% metal basis, the physical technique used was sonication in an ultrasonic bath for 6 h at a frequency of 43 kHz and a controlled temperature of not more than 20°C. When these steps were completed, the silver nanoparticles were dispersed in the base fluids, as per the data given in Table 1 (Hwang et al. (2008)).

Table 1 Summarizes the detailed experimental conditions of various silver nanofluid preparatory methods employed in this study.

Step	Method of producing silver nanofluid
1	Silver Nano powder < 100 nm particle size, 99.9% (metals basis) at concentrations of 0.5 wt% mixed with De-ionized water
2	Silver nanofluid Ultrasonic bath (Test condition Sonication time: 6 hrs. Frequency: 43 kHz.)

2.3 Heat transfer characteristics

The heat transfer efficiency of the RTPCT can be calculated from the temperature differences between the evaporator section and the condenser section. The total heat resistance can be calculated from the following equations (Kew and Reay (2006)):

$$Q_{Theoretical} = \frac{\Delta T}{Z_{total}} \quad (5)$$

$$\Delta T = \frac{(T_{h,in} - T_{c,out}) - (T_{h,out} - T_{c,in})}{\ln \frac{(T_{h,in} - T_{c,out})}{(T_{h,out} - T_{c,in})}} \quad (6)$$

Here, Z_{total} is the RTPCT's total heat resistance (see Figure 3), which is described as the TPCT's total heat resistance comprising the heat resistance components (Anon (1980)) $Z_1 - Z_{10}$

Z_1 and Z_9 are the heat resistors between the heat source and the external surface of the evaporator and between the external surface of the condenser and the heat source, respectively.

Z_2 and Z_8 are heat resistors for the heat conduction through the wall of the pipe in the evaporator and condenser parts, respectively.

Z_3 and Z_7 are the internal heat resistors of a boiling and condensed fluid, respectively.

Z_4 and Z_6 are the heat resistances at the contact surfaces between the vapor and the liquid at the evaporator and the condensation parts, respectively

Z_5 is the effective heat resistance caused by a pressure drop in the vapor that flows from the evaporator to the condenser.

Z_{10} is the thermal conductivity along the axis of the pipe wall. The surface area of RTPCT, which was more than that of TPCT, had full contact with the heat source and the heat releasing parts, as shown in Part C of Figure 2. The values created by RTPCT can be eliminated by Z_1 and Z_9 (see Figure 3).

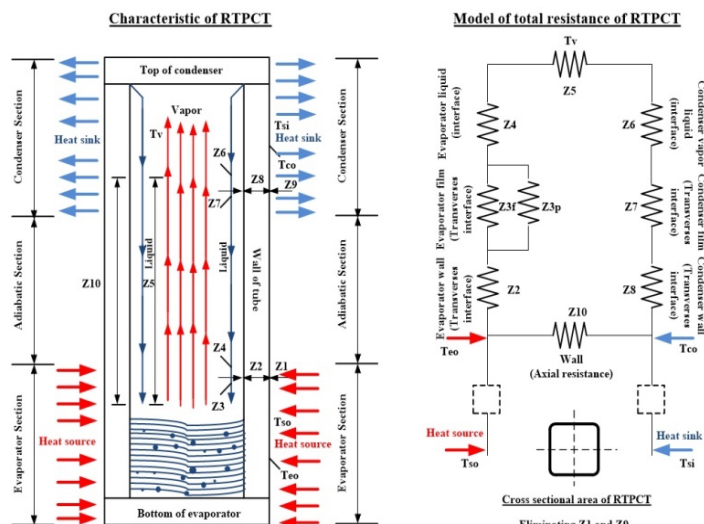


Fig. 3 The total heat resistance model of RTPCT

3. EQUIPMENT INSTALLATION AND ANALYSIS

Figure 4 shows the installation of test kits, which includes the formation of the RTPCT (see Figure 4 (a)). By connecting to a vacuum pump and beginning the process from vacuum within the RTPCT. Vacuum pump is connected to the valve of the substance addition kit. After the internal vacuuming process, the RTPCT feeds the working fluid through the addition tube, which is connected to the refill kit, as shown in Figure 4 (a). For the installation of the test kit (see Figure 4 (b)), hot water from the hot tub is sucked into the hot jacket using a pump to heat up the evaporator parts of the RTPCT. The hot water temperature from the hot tub is controlled by the control panel. The cold water from the cold bath was sent through the flow meter with 5% accuracy before entering the cold jacket. This was done to allow the cold water to reach the condensation section of the RTPCT. The system was equipped with nine temperature detection points. When the test system reached equilibrium under specified conditions, the flow patterns at the evaporator were recorded using a video camera. Concurrently, the data recordings of temperature were made for all the nine points using the K-type thermocouple with an uncertainty of 1.5°C; the thermocouple

was connected to a data logger (Yokogawa DX200) with 1°C accuracy. These nine measuring points consisted of two hot tubs, one hot water box, two thermal shields of the RTPCT, one cold-water inlet, one cold hot water outlet, one cold hot water tub, and one environmental temperature control system. Temperatures at the water outlet and inlet of the cold-water box were used to calculate the heat transfer rate. The RTPCT's wetted perimeter length was 25.2 mm along both the X and Y sides; the aspect ratio was 5, and NF was the working fluid. The filling ratio was 50% with respect to the evaporator volume, and the inlet water temperature at the condensing section of 0.25 L/min was 20°C; the test inclination angle was 90° from the horizontal plane, and the evaporator temperatures were 50°C, 70°C, and 90°C. This information is displayed in Table 2.

3.1 Test set installation and testing

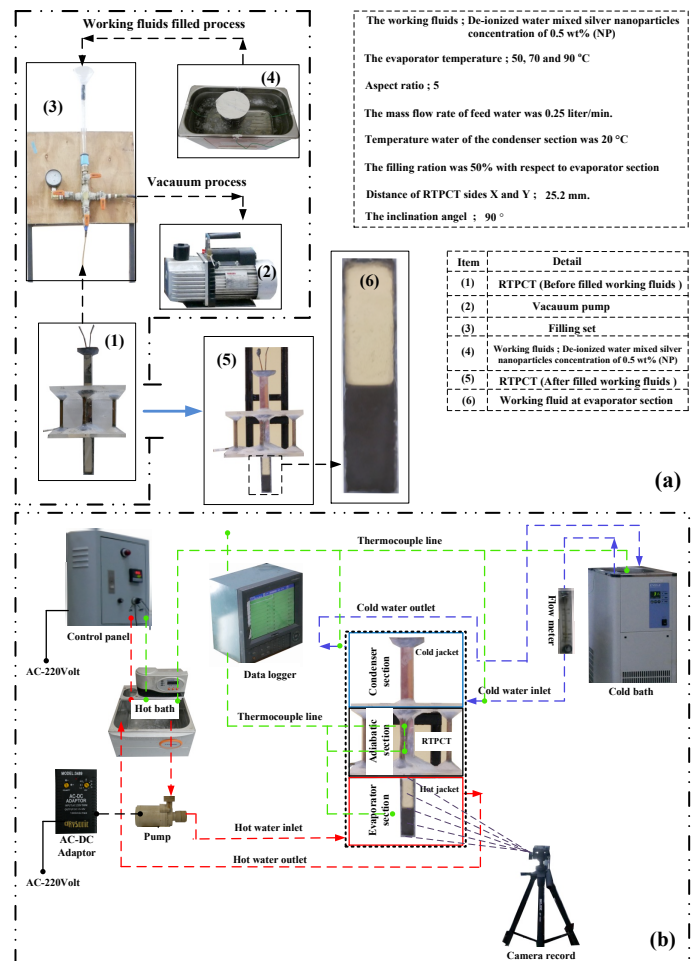


Fig. 4 Installation of test kits and tests

3.2 Heat transfer rate and heat flux

Heat transfer is initiated when the liquid state working fluid contained in the RTPCT received heat from a heat source that causes the liquid substances to boil, vaporize, and float through the heat shield to release the heat in the condenser. After being exposed to heat sources that had lower temperatures, the working fluid changes its status from vapor to liquid and flowed into the RTPCT evaporator because of gravity. The rate of heat transfer can be obtained from the following equation (Incropera and DeWitt (1996))

$$Q = m c_p (T_{co} - T_{ci}) \quad (7)$$

Table 2 Controlled and variable parameters.

Conditions	Details
Independent Variables	The evaporator temperature at 50, 70 and 90 °C (T_c)
Dependent Variables	- The effect of the evaporator temperature to the flow patterns two phase closed rectangular cross section area thermosyphon (RTPCT). - The effect of the evaporator temperature to heat transfer rate and heat flux two - phase closed rectangular cross section area thermosyphon (RTPCT).
Control Variables	- Distance of sides X and Y were 25.2 mm. (X, Y) - The working fluids; silver nanoparticles mixed with De-ionized water at concentration of 0.5 wt% (NF) - The inclination angle was 90°. (AI) - The mass flow rate of feed water was 0.25 liter/min. - The temperature water of the condenser section was 20 °C. (T_c) - The aspect ratios was 5 (AR)

Here, Q is the heat transfer rate (W), \dot{m} is the mass flow rate of water in the condenser section (kg/s), c_p is the specific heat capacity of the water (J/kg · °C), T_{co} is the water outlet temperature of the condenser section (°C), and T_{ci} is the water inlet temperature of the condenser section (°C).

The flow rate at the condenser can be calculated from the following equation:

$$\dot{m} = \rho v A \quad (8)$$

Where ρ is the density of the water (kg/m³), v is the velocity of the water (m/s), and A is the cross-sectional surface area of the water flow (m²).

The heat flux can be calculated from the following equation:

$$q = \frac{Q}{A_c} = \frac{Q}{\pi D_o L_c} \quad (9)$$

Here, q is the heat flux (W/m²), Q is the heat transfer rate (W), D_o is the outside diameter of the pipe (m), A_c is the external surface area of the condenser of the pipe (m²), and L_c is the length of the condenser of the pipe (m).

The behavior and flow patterns of the two phases that occurred in the evaporator parts of the RTPCT were recorded using video cameras from the beginning of the flow in each test case. Then, the recorded video was converted into still images at the rate of 60 frames/s. The two-phase flow patterns occurred as a continuous flow cycle; thus, the flow pattern percentage was calculated from three flow cycles of these recorded flows. The percentage of the flow pattern can be calculated by calculating the area (width × length) of each flow pattern as follows:

$$(\%) \text{ Each flow pattern} = \frac{\text{Number of grid for each flow pattern}}{\text{Total grid}} \times 100 \quad (10)$$

The grid with equal spacing of each channel is a fictional table that helps to estimate the location, distance, and area of an image. The two-

phase flow models obtained from this research are represented by a two-dimensional projection (width × length), which leads to the actual shape of each flow pattern for each angle and side.

3.3 Uncertainty Analysis

The uncertainty because of the calculation is of two types: Types A and B. Type A is the uncertainty caused by the sampling sources that are statistically evaluated. This can be calculated by the following equation:

$$\bar{X} = \frac{X_1 + X_2 + X_3 + \dots + X_n}{n_s} \quad (11)$$

Here, the standard deviation can be calculated from the following equation (12):

$$SD = \frac{\sqrt{(X_1 - \bar{X})^2 + (X_2 - \bar{X})^2 + (X_3 - \bar{X})^2 + \dots + (X_n - \bar{X})^2}}{n_s - 1} \quad (12)$$

$$u_{i,typeA} = \frac{SD}{\sqrt{n_s}} \quad (13)$$

Where n is the number of times measurements were made in the experiment.

Type B is the uncertainty caused by system errors that can be calculated from the following equation:

$$u_{i,typeB} = \frac{a}{\sqrt{3}} \quad (14)$$

Here, a is the semi-range (or half-width) between the upper and lower limits.

The sum of the standard uncertainty types (A and B) can be calculated from the following equation:

$$u_c = \sqrt{(u_{i,typeA})^2 + (u_{i,typeB})^2 + \dots etc} \quad (15)$$

Table 3 Uncertainty analysis result.

Type A	Type B		
Quantity source of uncertainty	Uncertainty of mean reading (°C)	Thermocouple type K (°C)	Data logger (°C)
Value of quantity		-200 – 1372	-200 – 1100
Confidence level (%)	95	95	95
Converge factor	2	2	2
Standard uncertainty (u_i)	0.00229	0.86602	0.57735
Sensitivity coefficient (c_i)	1	0.99817	0.99846
Uncertainty (u_{c_i})	0.00229	0.86443	0.57646
Combined uncertainty component	0.53073		
Expanded uncertainty	1.06146		

The expanded uncertainty can be calculated from the following equation:

$$U = Ku_c \quad (16)$$

When $k = 2$ is correct, the combined standard uncertainty in normally distributed results in the level of confidence is approximately 95 (Bell, (2001); Pipatpaiboon (2012)). The results of the uncertainty analysis of this study are given in Table 3.

For other coverage factors (normal distribution):

- K = 1 for a confidence level of approximately 68%,
- K = 2.5 for a confidence level of 99%, and
- K = 3 for a confidence level of 99.7%.

4. RESULTS AND DISCUSSION

According to the study of the flow patterns using NF as the working fluid within the RTPCT, the dimension of the X and Y sides was 25.2 mm, and the aspect ratio was 5. The inclination angle was 90° , and the testing evaporator temperatures were 50°C , 70°C , and 90°C .

4.1 Behavior and flow patterns within a rectangular two-phase closed thermosyphon

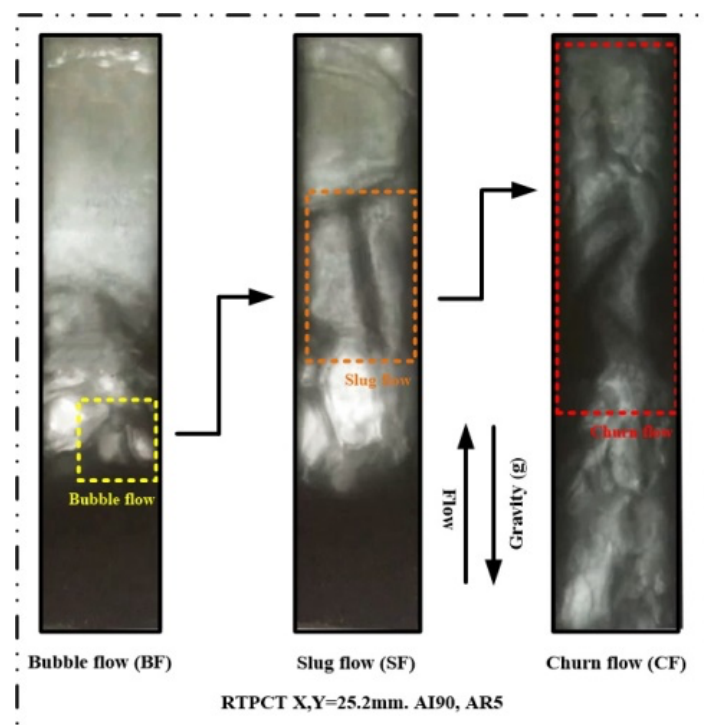


Fig. 5 The two phase flow pattern (RTPCT X, Y = 25.2 mm, AI 90° , AR5)

When the heat from the heat source comes into contact with the evaporator of the RTPCT, which contains the working fluid, the temperature of the pipe surface in the evaporator gradually rises to a level at which heat can penetrate through the pipe's wall to the working fluid, which results in the accumulated heat being absorbed by the working fluids. The working substance with the silver nanoparticles distributed in the base fluids increased the surface area for the heat receptor. Thus, the base fluids could be boiled easily. Silver nanoparticles have high conductivity; consequently, they can achieve efficient heat transfer to the base fluids. Therefore, the working fluid becomes a saturated liquid, which decreases its density and viscosity. Then, the working fluid begins to boil and change from the liquid state to the vapor state (see Figure 5). The initial characteristic of the BF formation begins with small vapor bubbles created by movements in the

Table 4 Effects of evaporator temperature on flow pattern within RTPCT with the lengths of the X and Y of 25.2 mm, the aspect ratio of 5, the inclination angle was 90° and the working fluids was de-ionized water mixed silver nanoparticles at the concentration of 0.5wt% (NF).

The evaporator temperature 90°C , ($q = 4.78\text{ kW/m}^2$)		
Churn flow	Slug flow	Bubble flow
% = 19.54 $V_g = 0.55\text{ m/s}$ $P = 3.81\text{ MPa}$	% = 9.28 $V_g = 0.47\text{ m/s}$ $P = 2.68\text{ MPa}$	% = 6.84 $V_g = 0.24\text{ m/s}$ $P = 1.35\text{ MPa}$
The evaporator temperature 70°C , ($q = 2.95\text{ kW/m}^2$)		
Churn flow	Slug flow	Bubble flow
% = 15.73 $V_g = 0.50\text{ m/s}$ $P = 2.84\text{ MPa}$	% = 9.28 $V_g = 0.47\text{ m/s}$ $P = 2.68\text{ MPa}$	% = 6.84 $V_g = 0.24\text{ m/s}$ $P = 1.35\text{ MPa}$
The evaporator temperature 50°C , ($q = 2.74\text{ kW/m}^2$)		
Churn flow	Slug flow	Bubble flow
% = 10.62 $V_g = 0.47\text{ m/s}$ $P = 2.02\text{ MPa}$	% = 6.51 $V_g = 0.44\text{ m/s}$ $P = 1.93\text{ MPa}$	% = 2.92 $V_g = 0.22\text{ m/s}$ $P = 0.96\text{ MPa}$

V_g , P = average speed (m/s) and average pressure (MPa) of the vapor bubble

fluid. The increase in the proportion of BF causes the steam bubbles to expand until they become bullet-shaped bubbles and form an SF pattern (Liu et al. (2007)). SF has a higher velocity than BF; thus, the bullet-shaped flow was distorted, and it started to break down. This type of flow is called turbulence flow. Certain SF heads may collide with the tails of the preceding lumps, which results in a type of flow called CF. Figure 5 shows that these flow patterns move upward to the condenser

for cooling down; they release heat and are condensed into a liquid before the liquid working fluid is pulled down along the inner surface of the pipe to the evaporator by the earth's gravity. Then, the working fluid accepts heat from the heat source and evaporates again. This is a typical work cycle of the working fluid within the RTPCT (Sichamnan, (2020); Terdtoon, (2001)).

4.2 Effect of evaporator temperature on two-phase flow patterns

The evaporation temperatures of 50°C, 70°C, and 90°C of the RTPCT were used with the wetted perimeter of the X and Y sides of 25.2 mm; the aspect ratio was 5, and the inclination angle was 90°. NF was the working fluid, which began to boil and evaporate in the saturated liquid state. When the evaporator temperature was 50°C (see Table 4), the three flow patterns, namely, BF, SF, and CF, which were found within the RTPCT, accounted for 2.92%, 6.51%, and 10.62% of the flow patterns, respectively. When the evaporator temperature was raised to 70°C, the three flow patterns within the RTPCT, namely, BF, SF, and CF, accounted for 6.87%, 9.28%, and 15.73% of the flow patterns, respectively. When the evaporator temperature was raised to 90°C, the working fluid boiled quite vigorously; the flow patterns generated in each cycle of the operation were more than those generated at the evaporation temperatures of 70°C and 50°C. Thus, the flow patterns were evidently higher at the evaporator temperature of 90°C than when the evaporator temperatures were 70°C and 50°C. At the evaporator temperature of 90°C, three forms of flow patterns, namely, BF, SF, and CF, were found, which accounted for 7.34%, 11.75%, and 19.54% of the flow patterns, respectively. When considered in conjunction with the pressure generated by the two flow patterns at different evaporator temperatures, the increased evaporator temperature resulted in vigorous and continuous boiling. The evaporator temperature directly affected the pressure giving rise to two flow patterns. At the evaporator temperatures of 90°C, 70°C, and 50°C, the pressure generated by CF and SF was high. The two flow patterns affected the heat transfer rate and heat flux. The maximum pressures at 90°C of the evaporator temperature for CF, lump flow, and BF were 3.81, 3.38, and 1.62 MPa, respectively. These two-phase flow patterns passed through the heat shield to the condenser where the temperature was low, and they began to release the heat. The two-phase flow consisted of the liquid and gas states; after releasing the heat, the liquid working fluid was pulled down by the earth's gravity along the inner surface of the pipe to the evaporator (Franco and Filippeschi (2012), Smith et al. (2016)).

4.3 Relationship of flow patterns, velocity, and heat flux

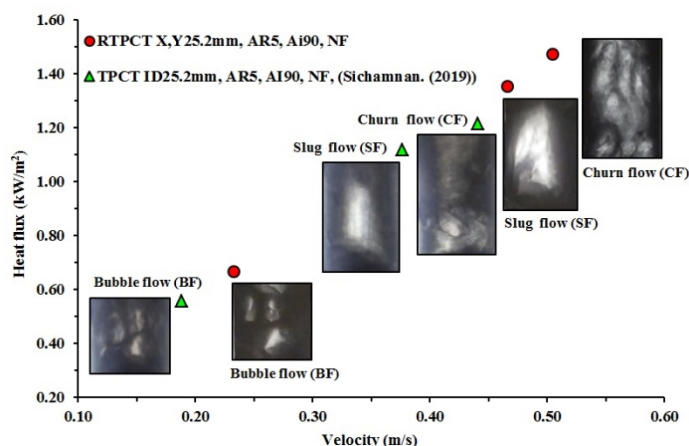


Fig. 6 Relationship of flow patterns velocity and heat flux of RTPCT which has the length of sides X and Y of 25.2 mm, and aspect ratio of 5

Figure 6 shows the relationship of the flow patterns, velocities, and heat flux values of the RTPCT with the wetted perimeter of 25.2 mm along the X and Y sides; the aspect ratio was 5, and the inclination angle was 90°; NF was the working fluid. The changing flow pattern was accompanied by the velocity and heat flux of each flow pattern. Depending on the flow cycle, BF was initiated by boiling, and its movements accumulated energy both in the form of heat and velocity. This resulted in the appearance or shape of the BF expanding with the movement, which finally enlarged and elongated the bubble sizes such that the flow resembled a bullet. This flow type is also known as SF. Because of the behaviors and characteristics of the velocity and pressure of the flow, which increased in accordance with the movement, the flow became turbulent and distorted. This led to a different type of flow called CF, as shown in Figure 6 (Liu et al. (2007), Payakaruk et al. (2020), Sichamnan. (2019)). The two-phase flows of the RTPCT resulted in high heat flux and intensity increasing from BF and SF to CF.

The velocity and behavior of the flow patterns were obtained by comparing the RTPCT flow with the TPCT flow. The wetted perimeter of the RTPCT was 25.2 mm along the X and Y sides, and it had an aspect ratio of 5. The TPCT had a diameter of 25.2 mm and an aspect ratio of 5. NF was used as the working fluid (Sichamnan. (2019)). The results are shown in Figure 6. The results prove that BF, SF, and CF obtained from the TPCT exhibited lower flow velocities than those obtained from the RTPCT. The RTPCT takes the form of a square rod with square cross-sectional areas for receiving heat at the evaporator and releasing the heat at the condenser. The area of the RTPCT was larger than that of the TPCT, as shown in Figure 2. The RTPCT possessed a larger wetted contact area between the working fluid and the inner pipe surface than the TPCT. Additionally, when the evaporator section of the RTPCT received heat from the heat source, its working fluid boiled easily, which resulted in faster two-phase flow patterns of BF, SF, and CF from the beginning. Additionally, in both the evaporator section and the condenser section, the RTPCT surface area was greater than the TPCT surface area. Thus, when the working fluid condensed at the condenser section, the condensed liquid film that was formed had enough space for distribution on the inner surface of the RTPCT. Consequently, the condensed liquid film was quite thin and spread out over the entire area. This helped to reduce the friction or the collision of the flow pattern that floated up from the evaporator section to the condenser section (Bhuwaketkumjohn and Parametthanuwat (2017), Srimuang et al. (2009)). With this flow behavior and the characteristics of the RTPCT condensation, BF, SF, and CF generated by the RTPCT had higher flow velocities than the ones generated by TPCT (see Figure 6).

4.4 Effects of the evaporator temperature on the heat flux

Figure 7 shows the relationship between the evaporator temperature and the heat flux obtained by testing the RTPCT with the wetted perimeter of 25.2 mm along the X and Y sides and the aspect ratio of 5; this heat flux was compared with the heat flux obtained from a TPCT with the diameter of 25.2 mm and the aspect ratio of 5 when NF was used as the working fluid (Sichamnan. (2019)).

When tested under the same conditions (see Figure 7), the results showed that the average heat flux obtained from the RTPCT was higher than the average heat flux obtained from the TPCT that used NF and deionized water as the working fluids. At the 90 °C evaporation section temperature test, the highest heat fluxes were found to be 4.78, 3.98, and 2.14 kW/m² for the cases evaluated with RTPCT, TPCT when NF was used as working fluid, and TPCT when deionized water was used as working fluid, respectively.

The RTPCT had larger surface areas at the evaporator and the condenser sections than the TPCT, as shown in Part C of Figure 2. Furthermore, when Part C of Figure 2 is considered in conjunction with Figure 3 (which shows the total heat resistance diagram of the RTPCT combined with the surface areas of the RTPCT in the evaporator and condenser parts), the heat resistance between the external surface of the

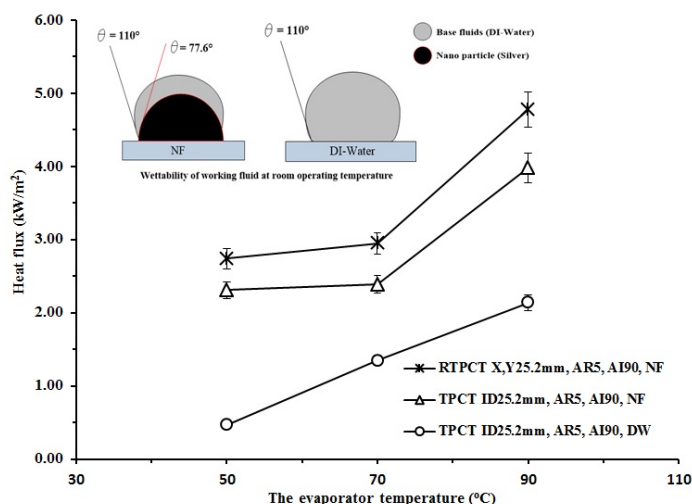


Fig. 7 Shows the relationship between evaporator temperature and the heat flux of RTPCT

evaporator and the heat source (Z1) and the heat resistance between the external surface of the condenser and the heat source (Z9) were both eliminated. This helped the working fluid to reach the boiling point in the evaporator section and easily release the heat at the condenser. When the evaporator temperature was high, the amount of heat received by the working fluid also increased. When the working fluid was in the form of a saturated liquid, its density and viscosity were reduced according to the rising temperature. The working fluid boiled vigorously and frequently as the temperature of the evaporator section increased, and the fluid changed from liquid to gas before floating to release the heat at the condenser section. Moreover, this research used the NF within the RTPCT, which further enhanced the heat transfer characteristics of the RTPCT. The silver nanoparticle fluid was suspended in the base fluid (deionized water), which helped increase the surface area or the contact angle to the heat of the base fluid much more than using just the base fluid. The results obtained are shown in Figure 7. Clearly, it was easier to boil the base fluid in the evaporator section when the fluid was combined with silver nanoparticles that had higher thermal conductivity than water. (Paramatthanuwat et al. (2010)). Therefore, the two-phase state flow patterns within the RTPCT were directly affected. The results obtained from Figure 6 and Table 4 were consistent with the velocity of the flow patterns from the RTPCT, which showed higher flow velocity than any patterns obtained from the TPCT. Consequently, changes in the flow patterns from BF to SF and CF could occur quite rapidly. This led to a greater percentage of occurrences of CF and SF. Due to the high percentages and velocities of CF and SF, these flow types could transfer and release more heat at the condenser section. The transfer capacity was proportionate to the occurrence of the flow patterns. Thus, the CF and SF directly affected the heat transfer in the RTPCT. The RTPCT, which used silver nanoparticles as the working fluid, had a higher average heat flux in all the test categories when compared with the results obtained from both types of TPCTs that used silver nanoparticles and water as the working fluid. The results obtained are shown in Figure 7.

5. CONCLUSIONS

- Tests conducted at the RTPCT's evaporation temperatures of 50°C, 70°C, and 90°C with the inclination angle of 90° and with NF as the working fluid revealed three flow patterns: BF, SF, and CF. SF and CF had relatively high occurrence percentages, and they affected the heat flux.
- A comparison of the behaviors and flow patterns obtained from the RTPCT and the TPCT showed that the velocity of

all the flow patterns obtained from the RTPCT was higher than the flow velocity obtained from TPCT (see Figure 6).

- As the evaporator temperature increased, the heat transfer per unit area or the heat flux also increased. The maximum heat flux in the RTPCT was 4.78 kW/m² at the evaporation temperature of 90 °C, and the heat flux values were 2.95 and 2.74 kW/m² for the evaporation temperatures of 70 °C and 50°C, respectively.
- When the RTPCT was altered by the geometric cross-sectional area, it was determined by the wetted perimeter expressed as the X and Y sides. For the TPCT, the geometric cross-sectional area was determined by the internal diameter. The nature of the transition was to a rectangular cross-sectional area, which resulted in a better contact surface exposure to heat sources and heat receivers. This enhanced the ability to eliminate the heat resistance between the heat source and the heat receiver. Thus, the total heat resistance in the RTPCT was less than that in the TPCT.
- To study the two-phase flow behavior and improve the thermal properties of the RTPCT, this research used NF as the working fluid within the RTPCT. A major advantage of silver nanoparticles is that they increase the contact surface area for receiving and releasing heat to the base fluids. Furthermore, silver nanoparticles facilitate the boiling of the base fluids when heated. This easily led to the two-state flow and a transition to another type of flow, which was accompanied by heat convection. This was caused by the higher thermal conductivity of the silver nanoparticles when compared with a base fluid used as a sole working fluid.

ACKNOWLEDGEMENTS

This research work was conducted at the Department of Mechanical Engineering, Faculty of Industry and Technology, Rajamangala University of Technology Isan, Sakon Nakhon Campus, Sakon Nakhon 47160, Thailand.

NOMENCLATURE

<i>RTPCT</i>	rectangular two-phase closed thermosyphon
<i>NF</i>	nanofluid
<i>TPCT</i>	two-phase closed thermosyphon
<i>BF</i>	bubble flow
<i>SF</i>	slug flow
<i>CF</i>	churn flow
V_g	speed of the vapor bubble (m/s)
P	pressure of the vapor bubble (MPa)
T	temperature (°C)
e	evaporator
c	condenser

REFERENCES

- Bhuwakietkumjohn, N., and Paramatthanuwat, T., 2017, "Heat transfer behaviour of silver particles containing oleic acid surfactant: application in a two phase closed rectangular cross sectional thermosyphon (RTPCT)," *International Journal of Heat and Mass Transfer*, 53(1), 37-48.
<https://doi.org/10.1007/s00231-016-1798-1>
- Kew, P. A., and Reay, D. A., 2006, *Heat pipes: theory, design and applications*, Butterworth – Heinemann.
<https://doi.org/10.1016/B978-0-7506-6754-8.X5000-3>
- Noie, S.H., Emamib, M.R.S., and Khoshnoodib, M., 2007, "Effect of inclination angle and filling ratio on thermal performance of a two-

phase closed thermosyphon under normal operating conditions,” *Heat Transfer Eng*, 28(4), 365-371.

<https://doi.org/10.1080/01457630601122997>

Rittidech, S., 2010, *Heat pipe technology*, 2nd ed., Maharakham University.

Moon, S.H., Moon, G., Ko, S.C., and Kim, Y.T., 2004, “Experimental study on the thermal performance of micro - heat pipe with cross-section of Polygon,” *Microelectronics Reliability*, 44, 315-321.

[https://doi.org/10.1016/S0026-2714\(03\)00160-4](https://doi.org/10.1016/S0026-2714(03)00160-4)

Amatachaya, P., and Srimuang, W., 2010, “Comparative heat transfer characteristics of a flat two phase closed thermosyphon (FTPCT) and a conventional two phase closed thermosyphon (CTPCT),” *International Communications in Heat and Mass Transfer*, 37, 293-298.

<https://doi.org/10.1016/j.icheatmasstransfer.2009.11.004>

Hussein, H., El-Ghetany, H., and Nada, S., 2006, “Performance of wickless heat pipe flat plate solar collectors having different pipes cross sections geometries and filling ratios,” *Energy conversion and management*, 47, 1539-1549.

<https://doi.org/10.1016/j.enconman.2005.08.009>

Srimuang, W., Rittidech, S., and Bubphachot, B., 2009, “Heat transfer characteristics of a vertical flat thermosyphon (VFT),” *Journal of mechanical science and technology*, 23(9), 2548-2554.

<https://doi.org/10.1007/s12206-009-0703-y>

Abdallah, Ayad S., Yasin, Nabil Jamil., and Ameen, Hani Aziz., 2022, “THERMAL PERFORMANCE ENHANCEMENT OF HEAT PIPE HEAT EXCHANGER IN THE AIR-CONDITIONING SYSTEM BY USING NANOFLUID.” *Frontiers in Heat and Mass Transfer (FHMT)*, 18(10), 1-10.

<http://dx.doi.org/10.5098/hmt.18.10>

Paramatthanuwat, T., Boothaisong, S., Rittidech, S., and Booddachan, K., 2010, “Heat transfer characteristics of a two-phase closed thermosyphon using deionized water mixed with silver nano,” *Heat and mass transfer*, 46(3), 281-285.

<https://doi.org/10.1007/s00231-009-0565-y>

Kang, S-W., Wei, W-C., Tsai, S-H., and Yang, S-Y., 2006, “Experimental investigation of silver nano-fluid on heat pipe thermal performance,” *Applied thermal engineering*, 26, 2377-2382.

<https://doi.org/10.1016/j.applthermaleng.2006.02.020>

Noie, S.H., Zeinali Heris, S., Kahani, M., and Nomee, S.M., 2009, “Heat transfer Enhancement using Al₂O₃/water nanofluid in a two-phase closed thermosyphon,” *Heat Fluid Flow*, 30, 700-705.

<https://doi.org/10.1016/j.ijheatfluidflow.2009.03.001>

Shin, D-R., Rhi, S-H., Lim, T-K., and Jang, J-C., 2011, “Comparative study on heat transfer characteristics of nanofluidic thermosyphon and grooved heat pipe,” *Journal of mechanical science and technology*, 25, 1391.

<https://doi.org/10.1007/s12206-011-0409-9>

Terdtoon, P., Chailungkar, M., and Shiraish, M., 1998, “Effects of aspect ratios on internal flow patterns of an inclined closed two-phase thermosyphon at normal operating condition,” *Heat transfer engineering*, 19, 75-85.

<https://doi.org/10.1080/01457639808939938>

Bhuwakietkumjohn, N., and Rittidech, S., 2010, “Internal flow patterns on heat transfer characteristics of a closed - loop oscillating heat-pipe with check valves using ethanol and a silver nano-ethanol mixture,” *Experimental Thermal and Fluid Science*, 34, 1000-1007.

<https://doi.org/10.1016/j.expthermflusci.2010.03.003>

Asirvatham, L.G., Wongwises., S, and Babu, J., 2015, “Heat transfer performance of a glass thermosyphon using graphene-acetone nanofluid,” *Journal of Heat Transfer*, 137.

<https://doi.org/10.1115/1.4030479>

Sichamnan, S., Chompookham, T., and Parametthanuwat, T., 2020, “A case study on internal flow patterns of the two-phase closed thermosyphon (TPCT),” *Case Studies in Thermal Engineering*, 100586.

<https://doi.org/10.1016/j.csite.2020.100586>

Srimuang, W., Amatachaya, P., and Krittacom, B., 2011, “Thermal performance of a flat two phase closed thermosyphon (FTPCT) with different cross-sectional areas and source temperatures,” In 10th international heat pipe symposium, Tamsui, New Taipei City, Taiwan, 147-152.

Hwang, Yujin., Lee, Jae-Keun., Lee, Jong-Ku., Jeong, Young-Man., Cheong, Seong-ir., Ahn, Young-Chull., and Kim, Soo H., 2008, “Production and dispersion stability of nanoparticles in nanofluids,” *Powder Technology*, 186, 145-153.

<https://doi.org/10.1016/j.powtec.2007.11.020>

Anon., 1980, *Heat pipes-general information on their use, operation and design*, Data Item No. 80013 Engineering Sciences Data Unit, London.

Incropera, F.P., DeWitt, D.P., 1996, *Fundamental of heat and mass transfer*, John Wiley & Sons, New York, NY, USA.

Bell, S. A., 2001, *A beginner's guide to uncertainty of measurement*.

Pipatpaiboon, N., Rittidech, S., and Meena, P., 2012, “Experimental study of a thermosyphon heat exchanger (TPHE) in a bio-diesel factory in Thailand,” *Arabian Journal for Science and Engineering*, 37, 2047-2060.

<https://doi.org/10.1007/s13369-012-0310-6>

Liu, S., Li, J., and Chen, Q., 2007 “Visualization of flow pattern in thermosyphon by ECT. In AIP Conference Proceedings,” *American Institute of Physics*, 914, 775-785.

<https://doi.org/10.1016/j.flowmeasinst.2007.06.012>

Terdtoon, P., 2001, *Boiling*, Chiang Mai University, Thailand.

Franco, A., and Filippeschi, S., 2012 “Closed loop two-phase thermosyphon of small dimensions: a review of the experimental results,” *Microgravity Science and Technology*, 24, 165-179.

<https://doi.org/10.1007/s12217-011-9281-6>

Smith, K., Siedel, S., Robinson, A. J., and Kempers, R., 2016, “The effects of bend angle and fill ratio on the performance of a naturally aspirated thermosyphon,” *Applied Thermal Engineering*, 101, 455-467.

<https://doi.org/10.1016/j.applthermaleng.2016.01.024>

Payakaruk, T., Terdtoon, P., and Rittidech, S., 2000, “Correlations to predict heat transfer characteristics of an inclined closed two-phase thermosyphon at normal operating conditions,” *Applied Thermal Engineering*, 20, 781-790.

[https://doi.org/10.1016/S1359-4311\(99\)00047-2](https://doi.org/10.1016/S1359-4311(99)00047-2)

Sichamnan, S., 2019, “Flow Patterns and Heat Transfer Characteristic of Two-Phase Closed Rectangular Cross Sectional Area Thermosyphon,” Doctor of Philosophy, Maharakham University, Thailand.